Scattering from Large-Scale Stratified Rough Surfaces using Improved BMIA/CAG

Linfeng He, Liang Lang, Qingxia Li, and Wenchao Zheng

Science and Technology on Multi-Spectral Information Processing Laboratory
Huazhong University of Science and Technology, Wuhan, 430074, China
linfeng_he@mail.hust.edu.cn, l_lang@mail.hust.edu.cn,
qingxia_li@mail.hust.edu.cn, wenchaozheng10@gmail.com

Abstract ─ A numerical method is presented to analyze the scattering behavior of large-scale stratified rough surfaces. The method improves the banded matrix iterative approach / canonical grid (BMIA/CAG) by adopting some simple formulas to calculate the coupling interactions between different surfaces. Such treatment reduces the complexity of the method at expense of little accuracy when the roughness of surfaces can be ignored compared to the distance between surfaces, and also reduces the computation time by parallel implementation technique. Based on emissivity calculation, the one-dimensional method is proven to be effective for the analysis of some scattering properties. Then the proposed method is compared with the method of moments (MoM) by example of multilayered lunar regolith. Details of numerical results are given and discussed, which provide a guide in the application of the improved method.

Index Terms ─ Banded matrix iterative approach / canonical grid method (BMIA/CAG), method of moments (MoM), remote sensing, rough surface scattering, stratified rough surfaces.

I. INTRODUCTION

Electromagnetic characteristics of stratified rough surfaces have been studied for many applications in remote sensing, such as lunar exploration [1, 2], buried objects detection [3, 4], ocean observation [5], etc. With the advent of modern computers, it is attractive to study scattering from rough surfaces with fast numerical methods [6].

Based on the method of moments (MoM), the Maxwell equations are converted into matrix equations which can be solved by linear iterative solvers [7]. For the case of stratified rough surfaces, main numerical methods include extended boundary condition method (EBCM) with truncated singular value decomposition (TSVD) [8], forward-backward spectral acceleration (FBSA) [9], the steeped descent fast multipole method (SDFMM) [10] and propagation-inside-layer expansion (PILE) [11] approach. The hybrids of these methods [12] and the parallel implementation technique [13] have been used in some methods to speed up computations. Nevertheless, the computational complexity of SVD in [8] increases rapidly with the size of the matrix; FBSA may fail to converge in lossless cases or for media with large permittivity [9]; the SDFMM requires a depth less than one free-space wavelength to satisfy the quasiplanar structure constraint [10]; the derivation of characteristic matrix of the layer [11] becomes prohibitively challenging when too many interfaces are involved. Besides, there are also some researches on scattering problem from stratified media with a perfect electric conductor (PEC) layer [14]. Their constraints limit the use of the methods for lunar regolith.

The banded matrix iterative approach on a canonical grid (BMIA/CAG) [15, 16] is an efficient method for one-dimensional (1-D) single surface because it requires low dynamic memory and computation time. A multilevel expansion method [16] has been used to improve the BMIA/CAG for surfaces with root mean square (rms) heights up to several wavelengths [17].

Submitted On: Dec. 7, 2011
Accepted On: March 4, 2012

However, for stratified rough surfaces, the expanding of coupling interactions between different surfaces is much more complicated than similar operations for a single surface case. The complexity of programming and calculations makes the BMIA/CAG inefficient.

To overcome this limitation, the BMIA/CAG method is improved and generalized to calculate the scattering from 1-D stratified rough surfaces in this paper. For convenience, the improved method is named as generalized BMIA (GBMIA) throughout the paper. In Section II, the principle of the BMIA/CAG is first investigated, and then simplified formulas for the GBMIA are introduced. With these simplifications, the solving of the linear matrix equation in the iterative approach is parallelizable and the computation can be accelerated by the parallel implementation technique, which is shown in Section III. More numerical results and discussion on different models are presented to prove the validity of the GBMIA in Section IV. Remarks are given in Section V.

II. FORMULATION

A. Integral equations

The geometry of 1-D stratified rough surfaces is illustrated in Fig. 1, with N rough surfaces, dividing the space into $N + 1$ layers. The j-th surface S_j is described by the profile $z = f_j(x)$, where $x \in [-L/2, L/2]$, L is the length of the surface. For the j-th layer V_j, the properties are expressed by the complex permittivity ε_j and the complex permeability μ_j, and the total field is denoted by ψ_j. Besides, for the j-th layer ($j = 1,\ldots,N$-1), let H_j denote the average thickness of the layer.

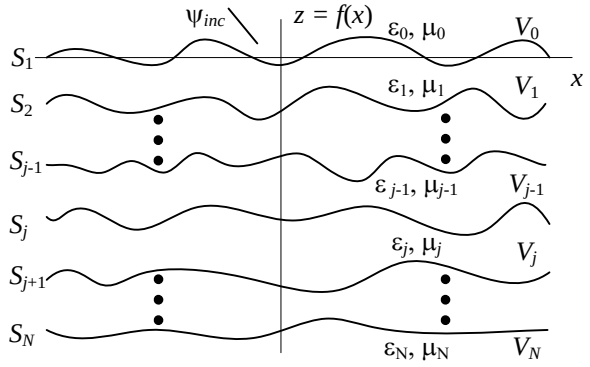

Fig. 1. Schematic diagram of 1-D stratified rough surfaces.

With an incident field ψ_{inc} impinging on S_0, the double integral equations for the j-th surface S_j can be written as

$$\begin{aligned}\frac{1}{2}\psi_j(\bar{\mathbf{r}}') - P.V.\int_{S_j} ds\,\psi_j(\bar{\mathbf{r}})\hat{\mathbf{n}}_j\cdot\nabla G_j(\bar{\mathbf{r}},\bar{\mathbf{r}}') \\ + \int_{S_j} ds G_j(\bar{\mathbf{r}},\bar{\mathbf{r}}')\hat{\mathbf{n}}_j\cdot\nabla\psi_j(\bar{\mathbf{r}}) \\ + \int_{S_{j-1}} ds\,\psi_{j-1}(\bar{\mathbf{r}})\hat{\mathbf{n}}_{j-1}\cdot\nabla G_j(\bar{\mathbf{r}},\bar{\mathbf{r}}') \\ - \int_{S_{j-1}} ds G_j(\bar{\mathbf{r}},\bar{\mathbf{r}}')\rho_{j,j-1}\hat{\mathbf{n}}_{j-1}\cdot\nabla\psi_{j-1}(\bar{\mathbf{r}}) = 0 \quad \bar{\mathbf{r}}'\in S_j\end{aligned} \tag{1}$$

$$\begin{aligned}-\frac{1}{2}\psi_j(\bar{\mathbf{r}}') - P.V.\int_{S_j} ds\,\psi_j(\bar{\mathbf{r}})\hat{\mathbf{n}}_j\cdot\nabla G_{j+1}(\bar{\mathbf{r}},\bar{\mathbf{r}}') \\ + \int_{S_j} ds G_{j+1}(\bar{\mathbf{r}},\bar{\mathbf{r}}')\rho_{j+1,j}\hat{\mathbf{n}}_j\cdot\nabla\psi_j(\bar{\mathbf{r}}) \\ + \int_{S_{j+1}} ds\,\psi_{j+1}(\bar{\mathbf{r}})\hat{\mathbf{n}}_{j+1}\cdot\nabla G_{j+1}(\bar{\mathbf{r}},\bar{\mathbf{r}}') \\ - \int_{S_{j+1}} ds G_{j+1}(\bar{\mathbf{r}},\bar{\mathbf{r}}')\hat{\mathbf{n}}_{j+1}\cdot\nabla\psi_{j+1}(\bar{\mathbf{r}}) = 0 \quad \bar{\mathbf{r}}'\in S_j\end{aligned} \tag{2}$$

where $\bar{\mathbf{r}}'$ is the position vector of the observation point on S_j and $\bar{\mathbf{r}}$ is that of the source point on the corresponding integral surface. G_j denotes the Green's function in V_j. *P.V.* represents the principal value integral. $\hat{\mathbf{n}}_j = \left(-f_j'(x)\hat{\mathbf{x}} + \hat{\mathbf{z}}\right)\Big/\sqrt{1+\left(f_j'(x)\right)^2}$, is the normal vector at $(x, f_j(x))$. $\rho_{j+1,j} = \mu_{j+1}/\mu_j$ for transverse electric (TE) wave and $\rho_{j+1,j} = \varepsilon_{j+1}/\varepsilon_j$ for transverse magnetic (TM) wave.

Specially, for the top surface S_1, i.e., $j = 1$, integrations on surface S_{j-1} in (1) become the incident field ψ_{inc}. For the bottom surface S_N, i.e., $j = N$, integrations on surface S_{j+1} in (2) go to zero. Thus, the scattering problem from stratified rough surfaces can be described by (1) and (2).

B. MoM implementation

According to the principle of MoM [18], each surface is divided equally into M segments of width $\Delta x = L/M$. Then the integral equations (1) and (2) can be discretized and converted to a linear matrix equation with the form $\overline{\overline{\mathbf{Z}}}\cdot\overline{\mathbf{X}} = \overline{\mathbf{b}}$, where $\overline{\overline{\mathbf{Z}}}$ is the coefficient matrix with $2MN \times 2MN$ elements, representing coupling interactions between observation and source points on surfaces; $\overline{\mathbf{b}}$ is a $2MN \times 1$ vector, representing incident fields on surfaces; and $\overline{\mathbf{X}}$ is a $2MN \times 1$ vector, denoting the surface unknowns to be solved.

For a scattering model with N rough surfaces, the coefficient matrix has the form of

$$\overline{\overline{\mathbf{Z}}} = \begin{bmatrix} \overline{\overline{\mathbf{Z}}}_1 & \overline{\overline{\mathbf{Z}}}_{21} & \overline{\overline{\mathbf{0}}} & \cdots & \overline{\overline{\mathbf{0}}} \\ \overline{\overline{\mathbf{Z}}}_{12} & \overline{\overline{\mathbf{Z}}}_2 & \overline{\overline{\mathbf{Z}}}_{32} & \ddots & \vdots \\ \overline{\overline{\mathbf{0}}} & \overline{\overline{\mathbf{Z}}}_{23} & \overline{\overline{\mathbf{Z}}}_3 & \ddots & \overline{\overline{\mathbf{0}}} \\ \vdots & \ddots & \ddots & \ddots & \overline{\overline{\mathbf{Z}}}_{N,N-1} \\ \overline{\overline{\mathbf{0}}} & \cdots & \overline{\overline{\mathbf{0}}} & \overline{\overline{\mathbf{Z}}}_{N-1,N} & \overline{\overline{\mathbf{Z}}}_N \end{bmatrix}_{2MN\times 2MN}, \quad (3)$$

where block matrices are

$$\overline{\overline{\mathbf{Z}}}_i = \begin{bmatrix} \overline{\overline{\mathbf{A}}}_{i-1,i} & \overline{\overline{\mathbf{B}}}_{i-1,i} \\ \rho_{i,i-1}\overline{\overline{\mathbf{A}}}_{i,i} & \overline{\overline{\mathbf{B}}}_{i,i} \end{bmatrix}_{2M\times 2M}, \quad i = 1, 2, ..., N,$$

$$\overline{\overline{\mathbf{Z}}}_{i+1,i} = \begin{bmatrix} \overline{\overline{\mathbf{0}}} & \overline{\overline{\mathbf{0}}} \\ \overline{\overline{\mathbf{C}}}_{i+1,i} & \overline{\overline{\mathbf{D}}}_{i+1,i} \end{bmatrix}_{2M\times 2M},$$

$$\overline{\overline{\mathbf{Z}}}_{i,i+1} = \begin{bmatrix} \rho_{i,i-1}\overline{\overline{\mathbf{C}}}_{i,i+1} & \overline{\overline{\mathbf{D}}}_{i,i+1} \\ \overline{\overline{\mathbf{0}}} & \overline{\overline{\mathbf{0}}} \end{bmatrix}_{2M\times 2M}, \quad i = 1, 2, ..., N\text{-}1.$$

$\overline{\overline{\mathbf{A}}}_{i,j}$, $\overline{\overline{\mathbf{B}}}_{i,j}$, $\overline{\overline{\mathbf{C}}}_{i,j}$, $\overline{\overline{\mathbf{D}}}_{i,j}$ are $M \times M$ block matrices. Elements in $\overline{\overline{\mathbf{A}}}_{i,j}$ and $\overline{\overline{\mathbf{C}}}_{i,j}$ have the similar form of (4), while those in $\overline{\overline{\mathbf{B}}}_{i,j}$ and $\overline{\overline{\mathbf{D}}}_{i,j}$ are in the form of (5). The details of expressions for these block matrices can be found in [11].

$$AC(m,n) = \Delta x \cdot H_0^{(1)}\left(k\left|\vec{\mathbf{r}}'_m - \vec{\mathbf{r}}_n\right|\right), \quad (4)$$

$$BD(m,n) = \Delta x \cdot \frac{ik}{4}\frac{H_1^{(1)}\left(k\left|\vec{\mathbf{r}}'_m - \vec{\mathbf{r}}_n\right|\right)}{\left|\vec{\mathbf{r}}'_m - \vec{\mathbf{r}}_n\right|} \times\left[f_n'(x_n)(x_n - x_m) - (f_n(x_n) - f_m(x_m))\right], \quad (5)$$

where k is the wave number in the corresponding layer. $H_0^{(1)}$ and $H_1^{(1)}$ are the zero-order and first-order Hankel functions of the first kind, respectively. An essential difference should be noticed that observation and source points are on the same surface for $\overline{\overline{\mathbf{A}}}_{i,j}$ and $\overline{\overline{\mathbf{B}}}_{i,j}$ while they are on different surfaces for $\overline{\overline{\mathbf{C}}}_{i,j}$ and $\overline{\overline{\mathbf{D}}}_{i,j}$.

C. BMIA/CAG method

The MoM solution is rigorous [19]. However, the memory requirements and computational complexity increase rapidly with the size of $\overline{\overline{\mathbf{Z}}}$. To this problem, the BMIA/CAG solves the matrix equation in an iterative approach, by decomposing each block matrix into two parts. For example, the matrix $\overline{\overline{\mathbf{A}}}$ is decomposed into

$$A^{(s)}(m,n) = \begin{cases} A(m,n) & |m-n| \le b_w \\ 0 & |m-n| > b_w \end{cases}, \quad (6)$$

and

$$A^{(w)}(m,n) = \begin{cases} 0 & |m-n| \le b_w \\ A(m,n) & |m-n| > b_w \end{cases}, \quad (7)$$

where $1 \le m, n \le M$, and b_w is an adjustable parameter and set to be $M/10$ in most cases [15]. Then $\overline{\overline{\mathbf{A}}}^{(s)}$ is a banded matrix which represents strong interaction and the remainder $\overline{\overline{\mathbf{A}}}^{(w)}$ represents the weak interaction part. $\overline{\overline{\mathbf{B}}}$, $\overline{\overline{\mathbf{C}}}$, $\overline{\overline{\mathbf{D}}}$ are decomposed in the same way. Then $\overline{\overline{\mathbf{A}}}^{(s)}$, $\overline{\overline{\mathbf{B}}}^{(s)}$, $\overline{\overline{\mathbf{C}}}^{(s)}$, $\overline{\overline{\mathbf{D}}}^{(s)}$ are grouped to be $\overline{\overline{\mathbf{Z}}}^{(s)}$, and others are separated into $\overline{\overline{\mathbf{Z}}}^{(w)}$.

The matrix equation becomes $\left[\overline{\overline{\mathbf{Z}}}^{(s)} + \overline{\overline{\mathbf{Z}}}^{(w)}\right]\overline{\mathbf{X}} = \overline{\mathbf{b}}$ which can be solved by the following iteration [18]

$$\overline{\overline{\mathbf{Z}}}^{(s)}\overline{\mathbf{X}}^{(p+1)} = \overline{\mathbf{b}}^{(p)}, \quad (8)$$

where $\overline{\mathbf{b}}^{(p)}$ represents the updated right-hand side with

$$\overline{\mathbf{b}}^{(0)} = \overline{\mathbf{b}}, \quad (9)$$

$$\overline{\mathbf{b}}^{(p)} = \overline{\mathbf{b}} - \overline{\overline{\mathbf{Z}}}^{(w)}\overline{\mathbf{X}}^{(p)}. \quad (10)$$

The stopping criterion for the iterative procedure is defined as $\sqrt{\left\|\overline{\mathbf{b}}^{(p+1)} - \overline{\mathbf{b}}^{(p)}\right\| \Big/ \left\|\overline{\mathbf{b}}^{(0)}\right\|} \times 100\%$.

In the BMIA/CAG, the solution to (8) can be solved by taking advantage of the sparsity of $\overline{\overline{\mathbf{Z}}}^{(s)}$, without inversing the full matrix $\overline{\overline{\mathbf{Z}}}$. $\overline{\overline{\mathbf{Z}}}^{(w)}$ is decomposed so that $\overline{\overline{\mathbf{Z}}}^{(w)}\overline{\mathbf{X}}^{(p)}$ product can be computed by the fast Fourier transform (FFT), which can avoid the storage of $\overline{\overline{\mathbf{Z}}}^{(w)}$, besides saving the CPU time [18].

D. Decomposition of $\overline{\overline{\mathbf{Z}}}^{(w)}$

To apply the FFT to $\overline{\overline{\mathbf{Z}}}^{(w)}\overline{\mathbf{X}}^{(p)}$ product, the $\overline{\overline{\mathbf{Z}}}^{(w)}$ needs to be decomposed in further into a sum of

$$\overline{\overline{\mathbf{Z}}}^{(w)} = \sum_i^{N_Z} \overline{\overline{\mathbf{Z}}}_i^{(w)}, \quad (11)$$

where $\overline{\overline{\mathbf{Z}}}_i^{(w)}$ has the form of $\overline{\overline{\mathbf{T}}}_m\overline{\overline{\mathbf{Z}}}_d\overline{\overline{\mathbf{T}}}_n$. $\overline{\overline{\mathbf{T}}}_m$ is a function of m, and $\overline{\overline{\mathbf{T}}}_n$ is a function of n. $\overline{\overline{\mathbf{Z}}}_d$ is a translationally invariant matrix [18]. N_Z is the number of such matrix.

The decomposition in (11) is equivalent to expand the Hankel functions in (4) and (5) in Taylor series at $z_d = z_0$. For elements in $\overline{\overline{\mathbf{A}}}^{(w)}$,

$$H_0^{(1)}\left(k\sqrt{x_d^2 + z_d^2}\right) = \sum_{t=0}^{N_T} a_t(x_d)\cdot\left(\frac{z_d^2 - z_0^2}{x_d^2}\right)^t, \quad (12)$$

where $x_d = |m\text{-}n|\Delta x$ is the horizontal distance between the observation and source points, and z_d is the vertical component. N_T is the number of Taylor terms truncated in numerical calculations.

For $\overline{\overline{\mathbf{A}}}$, all the observation and source points are on the same surface, and z_d is only affected by roughness of the surface. In this case, $z_0 = 0$. By substituting z_d with $f_m(x) - f_n(x)$, the second Taylor term ($t = 1$) in (12), for example, can be written as

$$a_1(x_d)\cdot\left(\frac{z_d}{x_d}\right)^2 = f_m^2(x)\frac{a_1(x_d)}{x_d^2} + 2f_m(x)\frac{a_1(x_d)}{x_d^2}f_n(x) + \frac{a_1(x_d)}{x_d^2}f_n^2(x) \quad . \quad (13)$$

Now, each item on the right side of (13) has the form of $T_m Z_d T_n$, where T_m and T_n are functions of m and n, respectively, and Z_d is only related to $|m-n|$. Let $N(t)$ denote the number of items with the form of $F_m Z_d F_n$ from the t-th Taylor term, then

$$N_Z = \sum_{t=0}^{N_T} N(t)\cdot \quad (14)$$

The decomposition of $\overline{\overline{\mathbf{B}}}^{(w)}$ is similar to that of $\overline{\overline{\mathbf{A}}}^{(w)}$. However, in case of stratified rough surfaces, The decompositions of $\overline{\overline{\mathbf{C}}}^{(w)}$ and $\overline{\overline{\mathbf{D}}}^{(w)}$ are quite more complex for that the observation and source points are on different surfaces and the Hankel functions should be expanded at $z_0 = H_i$ which is the distance between two surfaces. If the first three Taylor terms are used in numerical calculation, N_Z for $\overline{\overline{\mathbf{A}}}^{(w)}$, $\overline{\overline{\mathbf{B}}}^{(w)}$, $\overline{\overline{\mathbf{C}}}^{(w)}$ and $\overline{\overline{\mathbf{D}}}^{(w)}$ is 9, 27, 21, and 63, respectively. In single surface case, the total number N_Z in BMIA/CAG is 36, while the number will reach to 120 for stratified rough surfaces; and the complexity will grow with more Taylor terms.

E. Generalized BMIA

To reduce the complexity in decomposition of $\overline{\overline{\mathbf{C}}}^{(w)}$ and $\overline{\overline{\mathbf{D}}}^{(w)}$, some simpler formulas for $\overline{\overline{\mathbf{C}}}^{(w)}$ and $\overline{\overline{\mathbf{D}}}^{(w)}$ are introduced for special applications, which generalizes the BMIA/CAG method so as to study the scattering behavior of stratified rough surfaces.

The vertical component z_d for $\overline{\overline{\mathbf{C}}}$ and $\overline{\overline{\mathbf{D}}}$ can be written as

$$\begin{aligned} z_d &= H_i + \delta f(x_m) + \delta f(x_n) \\ &= H_i\left(1 + \frac{\delta f(x_m) + \delta f(x_n)}{H_i}\right), \end{aligned} \quad (15)$$

where $\delta f(x_m)$ and $\delta f(x_n)$ represent the distances of the observation point and source point to their mean surfaces, respectively.

In many applications, values of $\delta f(x_m)$ and $\delta f(x_n)$ can be ignored compared to H_i. For example, at the Mare Serenitatis on the Moon, the depth of lunar subsurface can reach several kilometers, while the rms height of the surface is only about one meter [20]. Let $z_d \approx H_i$, then

$$H^{(1)}\left(k\sqrt{x_d^2 + z_d^2}\right) \approx H^{(1)}\left(k\sqrt{x_d^2 + H_i^2}\right). \quad (16)$$

Now, the Hankel function in (16) only depends on x_d, so elements in the matrix on the same diagonal are the same. Then $\overline{\overline{\mathbf{C}}}$ and $\overline{\overline{\mathbf{D}}}$ are known as Toeplitz matrices.

In the GBMIA, the decomposing to $\overline{\overline{\mathbf{A}}}$ and $\overline{\overline{\mathbf{B}}}$ is the same as that done in the BMIA/CAG. For $\overline{\overline{\mathbf{C}}}$ and $\overline{\overline{\mathbf{D}}}$, observation and source points are on different surfaces. Taking the thickness of layers into account, the whole matrices $\overline{\overline{\mathbf{C}}}$ and $\overline{\overline{\mathbf{D}}}$ are considered as weak part, i.e. $\overline{\overline{\mathbf{C}}}^{(w)} = \overline{\overline{\mathbf{C}}}$ and $\overline{\overline{\mathbf{D}}}^{(w)} = \overline{\overline{\mathbf{D}}}$, the product of which and vector can be computed by the FFT directly. Now the number N_Z for $\overline{\overline{\mathbf{C}}}^{(w)}$ or $\overline{\overline{\mathbf{D}}}^{(w)}$ is only one, which is greatly reduced.

In GBMIA, the strong part $\overline{\overline{\mathbf{Z}}}^{(s)}$ for stratified rough surfaces is now reduced to

$$\overline{\overline{\mathbf{Z}}}^{(s)} = \begin{bmatrix} \overline{\overline{\mathbf{Z}}}_1^{(s)} & \overline{\overline{\mathbf{0}}} & \cdots & \overline{\overline{\mathbf{0}}} \\ \overline{\overline{\mathbf{0}}} & \overline{\overline{\mathbf{Z}}}_2^{(s)} & \ddots & \vdots \\ \vdots & \ddots & \ddots & \overline{\overline{\mathbf{0}}} \\ \overline{\overline{\mathbf{0}}} & \cdots & \overline{\overline{\mathbf{0}}} & \overline{\overline{\mathbf{Z}}}_N^{(s)} \end{bmatrix}. \quad (17)$$

From the form of $\overline{\overline{\mathbf{Z}}}^{(s)}$ in (17), the solving to (8) can be divided into N linear equations with coefficient matrices $\overline{\overline{\mathbf{Z}}}_i^{(s)}$, which are sparse banded matrices with small scale. What's more, these equations are independent with each other, so solving to them can be implemented in parallel, which is helpful to save the computation time.

Let $\overline{\mathbf{X}} = [\overline{\mathbf{X}}_1^T, \overline{\mathbf{X}}_2^T, ..., \overline{\mathbf{X}}_{2N}^T]^T$, and $\overline{\mathbf{b}} = [\overline{\mathbf{b}}_1^T, \overline{\mathbf{b}}_2^T, ..., \overline{\mathbf{b}}_{2N}^T]^T$, the updating equations to (8) are

$$\overline{\mathbf{b}}_1^{(p+1)} = \overline{\boldsymbol{\psi}}_{inc} - \overline{\overline{\mathbf{A}}}_{0,1}^{(w)}\overline{\mathbf{X}}_1^{(p)} - \overline{\overline{\mathbf{B}}}_{0,1}^{(w)}\overline{\mathbf{X}}_2^{(p)}, \quad (18)$$

$$\overline{\mathbf{b}}_{2n}^{(p+1)} = \overline{\mathbf{0}} - \rho_{n,n-1}\overline{\overline{\mathbf{A}}}_{n,n}^{(w)}\overline{\mathbf{X}}_{2n-1}^{(p)} - \overline{\overline{\mathbf{B}}}_{n,n}^{(w)}\overline{\mathbf{X}}_{2n}^{(p)} - \overline{\overline{\mathbf{C}}}_{n+1,n}\overline{\mathbf{X}}_{2n+1}^{(p)} - \overline{\overline{\mathbf{D}}}_{n+1,n}\overline{\mathbf{X}}_{2n+2}^{(p)},$$

$$n = 1, 2, ..., N\text{-}1, \quad (19)$$

$$\overline{\mathbf{b}}_{2n+1}^{(p+1)} = \overline{\mathbf{0}} - \rho_{n,n-1}\overline{\overline{\mathbf{C}}}_{n,n+1}\overline{\mathbf{X}}_{2n-1}^{(p)} - \overline{\overline{\mathbf{D}}}_{n,n+1}\overline{\mathbf{X}}_{2n}^{(p)} - \overline{\overline{\mathbf{A}}}_{n,n+1}^{(w)}\overline{\mathbf{X}}_{2n+1}^{(p)} - \overline{\overline{\mathbf{B}}}_{n,n+1}^{(w)}\overline{\mathbf{X}}_{2n+2}^{(p)},$$

$$n = 1, 2, ..., N\text{-}1, \quad (20)$$

$$\overline{\mathbf{b}}_{2N}^{(p+1)} = \overline{\mathbf{0}} - \rho_{N,N-1}\overline{\overline{\mathbf{A}}}_{N,N}^{(w)}\overline{\mathbf{X}}_{2N-1}^{(p)} - \overline{\overline{\mathbf{B}}}_{N,N}^{(w)}\overline{\mathbf{X}}_{2N}^{(p)}. \quad (21)$$

III. EFFICIENCY EVALUATION

Memory requirement and computation time are two important criterions to assess a numerical method. The memory requirement depends on the number of non-zero elements in $\overline{\overline{\mathbf{Z}}}$. For the MoM, $\overline{\overline{\mathbf{Z}}}$ is a full matrix containing $4(2N\text{-}1)M^2$ elements, which will all be calculated and stored. In the BMIA/CAG, only non-zero elements in $\overline{\overline{\mathbf{Z}}}^{(s)}$ is necessary, the number of which is equal to $4(2N\text{-}1)[M+(b_w\text{-}1)(2M\text{-}b_w)]$. In the GBMIA, the number of non-zero elements in $\overline{\overline{\mathbf{Z}}}^{(s)}$ decreases to $4N[M+(b_w\text{-}1)(2M\text{-}b_w)]$. For the sake of illustration, the comparison of these three methods for different surface number N is listed in Table 1, with $M = 1000$, $b_w = M/10$.

Table 1: Number of non-zero elements (in million)

N	MoM	BMIA/CAG	GBMIA
1	4	0.7564	0.7564
2	12	2.2692	1.5128
3	20	3.782	2.2692
4	28	5.2948	3.0256
5	36	6.8076	3.782
6	44	8.3204	4.5384
7	52	9.8332	5.2948
8	60	11.346	6.0512
9	68	12.8588	6.8076
10	76	14.3716	7.564

From Table 1, the number of non-zero elements in GBMIA need to be calculated and stored is the least. When $N = 3$, the number to be stored in the GBMIA is only about 11% of that in the MoM, and 60% of that in the BMIA/CAG, which is a considerable saving in memory requirement and matrix filling time. This advantage becomes more obvious as N increases. The same conclusion can be obtained for different values of M.

To avoid the complexity of implementing BMIA/CAG for stratified rough surfaces, we evaluate the computation time of GBMIA and BMIA/CAG by two parameters: asymptotic convergence rate (R) [21] and time per iteration (T). For $\left[\overline{\overline{\mathbf{Z}}}^{(s)}+\overline{\overline{\mathbf{Z}}}^{(w)}\right]\cdot\overline{\mathbf{X}}=\overline{\mathbf{b}}$, the iteration matrix is defined as

$$\overline{\overline{\mathbf{Q}}}=\left(\overline{\overline{\mathbf{Z}}}^{(s)}\right)^{-1}\cdot\overline{\overline{\mathbf{Z}}}^{(w)}. \tag{22}$$

For the iterative approach to converge, the spectral radius of $\overline{\overline{\mathbf{Q}}}$ must be less than 1, i.e. $\rho\left(\overline{\overline{\mathbf{Q}}}\right)<1$. Then the asymptotic convergence rate is $R=-\log_{10}\left(\rho\left(\overline{\overline{\mathbf{Q}}}\right)\right)$, and the speedup (G) in computation time is evaluated by the ratio of the product of $1/R$ and T in BMIA/CAG over that in GBMIA. For several pairs of N and M, GBMIA and BMIA/CAG are compared on a standard personal computer with MATLAB, and values of R and T are shown in Table 2.

Table 2: Computation time evaluation

N	*M*	BMIA/CAG		GBMIA		*G*
		R	*T* (sec.)	*R*	*T* (sec.)	
2	600	0.35	0.7430	0.34	0.3958	1.82
	900	0.51	3.9665	0.47	0.7310	5.00
	1200	0.57	6.3811	0.47	1.2227	4.30
3	600	0.34	1.5818	0.31	0.5051	2.86
	900	0.49	5.4874	0.33	0.8420	4.39
	1200	0.50	17.055	0.30	1.5145	6.76
4	600	0.37	2.5300	0.31	0.6739	3.15
	900	0.33	10.488	0.30	1.1253	8.47
	1200	--	93.196	--	1.7155	--

From Table 2, due to the simplifications in $\overline{\overline{\mathbf{Z}}}^{(s)}$, the convergence rate decreases a little in GBMIA. However, there is a significant reduce in the time per iteration. As a result, the computation time in GBMIA is improved, and the overall speedup increases with N and M. When $N = 4$ and $M = 900$, the speedup reaches about 8.47.

For the case of $N = 4$ and $M = 1200$, although the convergence rate cannot be calculated with our computer, there is a surprising improvement on the time per iteration. Besides the utility of the parallel calculation in GBMIA, immoderate memory consuming in BMIA/CAG is also an important factor affecting the computation time.

These results show that GBMIA is more efficient and suitable for studying scattering problem of large-scale stratified surfaces.

IV. NUMERICAL RESULTS

The solution of surface integral equations obtained by using the MoM has been the standard for checking the validity of other numerical approaches [22]. In this section, the multilayered lunar regolith is taken as an example of stratified

rough surfaces. Before the verification of the GBMIA with MoM, it is necessary to verify that surface emissivity calculated by MoM with 1-D surface model is reliable.

A. Validation of MoM

In [1], the reflectivity for Monte Carle (MC) realized two-dimensional (2-D) lunar surface is calculated with the observation direction of 0°, and the average reflectivity of ten MC realizations in total is 0.0619 in TE case. To validate the MoM solutions, a simple two-layer model composed of free space and lunar soil, with $\mu_1 = \mu_0$, and $\varepsilon_1 = 2.7+0.01i$ in [1] is used here.

In this simulation, $L = 200\lambda$, where λ is the wavelength. A Thorsos tapered wave [23] is chosen as the incident wave, with $g = L/8$. The interface between free space and lunar soil is a Gaussian rough surface, with a small rms height of $h = 0.04\lambda$ and the correlation length of $l = 0.4\lambda$, in order that the surface emissivity obtained by the MoM can also be compared with the analytical small perturbation method (SPM) solution. Emissivities of the 1-D lunar model obtained at different incident angles are plotted in Fig. 2. The MoM has a good agreement with SPM solutions on a wide range of incident angles, in both TE and TM case.

As indicated in Fig. 2, the emissivity at the direction of 0° in TE case is 0.9331, which is corresponding to the reflectivity of 0.0669, very close to 0.0619 in [1]. Although some phenomena, such as depolarization are inherently for 2-D rough surface and cannot be observed using 1-D methods [19], the comparison indicates that 1-D method is still efficient to analyze scattering behavior, such as emissivity.

B. GBMIA comparison with MoM

Different models are now considered to compare the GBMIA method with the MoM. The emissivity calculated by GBMIA is denoted by e_{GBMIA}, and that obtained from the MoM is e_{MoM}. The relative error $|e_{\mathrm{GBMIA}} - e_{\mathrm{MoM}}|/e_{\mathrm{MoM}}$ is used to assess the accuracy of the proposed method. In this paper, attentions are given to the efficiency of

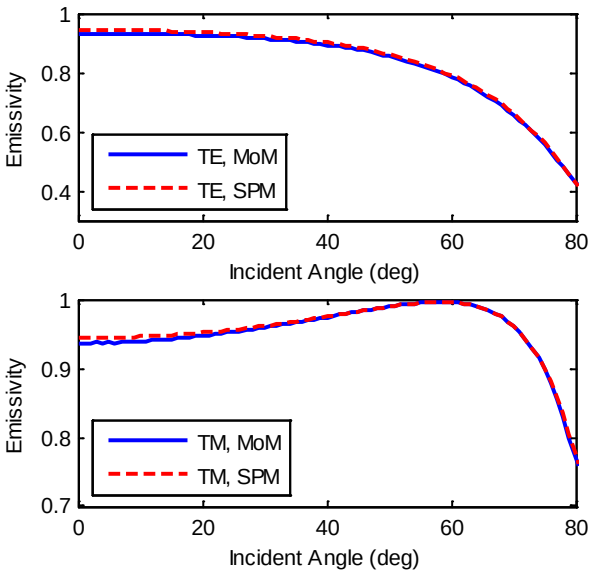

Fig. 2. Comparison of emissivity between MoM and SPM.

the GBMIA on multilayered medium, and the improvement by the multilevel expansion method for large rms heights will not be addressed here.

In this example, a three-layer model is used, composed of free space, lunar soil, and lunar rock, with $\mu_1 = \mu_2 = \mu_0$, and $\varepsilon_1 = 2.42*(1+0.00486i)$, $\varepsilon_2 = 7.8*(1+0.056i)$ [24]. $L = 40\lambda$, and the incident angle is 30°. Two interfaces are both Gaussian rough surfaces with the same roughness parameters. The correlation length $l = \lambda$, and different rms heights h (0, 0.1λ, 0.2λ, 0.3λ) are considered. The layer thickness H varies from λ to 30λ, and 20 realizations are generated for each thickness. The first three Taylor expansion terms are used and the residual error is set at 0.01.

The emissivity errors of GBMIA are shown in Fig. 3 for the TM case. From these curves, the emissivities of GBMIA are exactly the same as that of MoM for flat surfaces. For rough surfaces, the error diminishes as a whole, with H increasing, despite some small undulations; and the error decreases more quickly for surfaces with smaller rms height. For this three-layer model, the relative emissivity error by the GBMIA can be controlled below 1% when the thickness of lunar soil reaches 12λ.

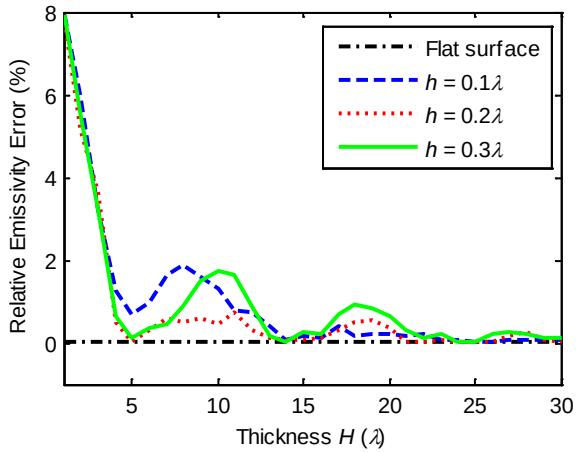

Fig. 3. Relative emissivity error between GBMIA and MoM for three-layer model versus the thickness of layer.

Ice deposits at the Lunar South Pole is an issue of diversity [2]. To estimate effects of possible ice deposit on scattering from lunar regolith, a lunar model containing ice is necessary. As an example to validate the GBMIA for a four-layer model, a layer of ice, with the permittivity of 3.2*(1+0.0035i) [24], is added between the lunar soil and rock layers. For different thicknesses of lunar soil (H_1 = 5λ, 10λ, 15λ, 20λ, 25λ, 30λ), the thickness of ice (H_2) changes from λ to 30λ. The rms height of surfaces is chosen as 0.1λ, and other parameters are the same as before. The errors for TM case are plotted in Fig. 4. In general, the error decreases with the increasing of H_1 and H_2, and the thickness of upper layer are more important on accuracy than that of lower layer. When the thickness of lunar soil is larger than 10λ, the error will not exceed 1% even with a thin ice layer.

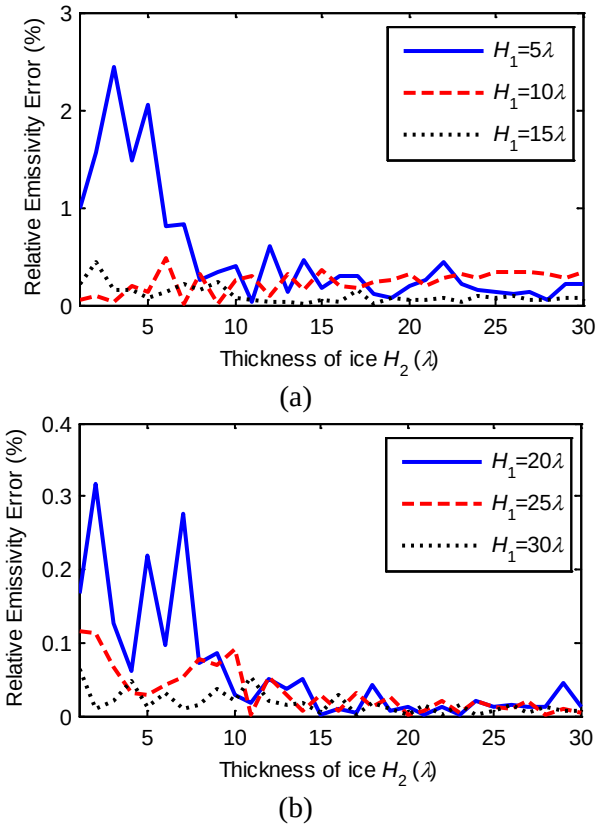

Fig. 4. Relative emissivity error between GBMIA and MoM for four-layer model versus different layer thickness: (a) H_1 = 5λ, 10λ, 15λ; (b) H_1 = 20λ, 25λ, 30λ.

V. CONCLUSION

The BMIA/CAG method is improved and generalized to investigate the electromagnetic scattering from large-scale stratified rough surfaces in case that the distance between two surfaces is very large compared to the roughness.

Comparing to the original BMIA/CAG, the GBMIA method reduces the complexity of decomposing coupling interactions between points on different surfaces. With the reduction, there is a good memory saving in the GBMIA. What's more important, the coefficient matrix in the GBMIA is a block diagonal matrix, and the solving to the matrix equation can be parallelizable. With the parallel implementation technique, the GBMIA has a significant speedup in computation time. These advantages make the GBMIA be suitable for applications in large-scale problems of stratified rough surfaces scattering.

With simplified formulas, the computational error is unavoidable. In numerical simulations, the MoM solution is first shown to be reliable on emissivity calculation. Then, the accuracy of the GBMIA is estimated by comparisons with the MoM, taking the multilayered lunar regolith as an example. The calculated relative emissivity error is below 1%, when the thickness of lunar soil is larger than about twelve free-space wavelengths.

Although only lunar models are used in numerical simulations, the proposed method can be used for other applications with similar structures.

ACKNOWLEDGMENT

This work was supported in part by the National High Technology Research and Development Program of China (863 Program) under Grant 2010AA122204, and in part by the National Natural Science Foundation of China under Grant 41001195.

REFERENCES

[1] Y. Q. Jin, and W. Z. Fa, "The Modeling Analysis of Microwave Emission from Stratified Media of Nonuniform Lunar Cratered Terrain Surface for Chinese Chang-E 1 Observation," *IEEE Geosci. Remote Sens. Lett.*, vol. 7, no. 3, pp. 530-534, Jul. 2010.

[2] W. G. Zhang, J. S. Jiang, H. G. Liu, X. H. Zhang, D. H. Zhang, D. H. Li, and C. D. Xu, "Distribution and Anomaly of Microwave Emission at Lunar South Pole," *Sci. China Earth Sci.*, vol. 53, no. 3, pp. 465-474, Mar. 2010.

[3] F. Delbary, K. Erhard, R. Kress, R. Potthast, and J. Schulz, "Inverse Electromagnetic Scattering in a Two-Layered Medium with an Application to Mine Detection," *Inverse Probl.*, vol. 24, no. 1, pp. 015002-1, Feb. 2008.

[4] K. P. Prokopidis and T. D. Tsiboukis, "Modeling of Ground-Penetrating Radar for Detecting Buried Objects in Dispersive Soils," *Appl. Comput. Electromagn. Soc. J.*, vol. 22, no. 2, pp. 287-294, Jul. 2007.

[5] O. Kilic, "A Discrete Random Medium Model for Electromagnetic Wave Interactions with Sea Spray," *Appl. Comput. Electromagn. Soc. J.*, vol. 23, no. 3, pp. 286-291, Sep. 2008.

[6] L. Zhou, L. Tsang, V. Jandhyala, Q. Li, and C. H. Chan, "Emissivity Simulations in Passive Microwave Remote Sensing with 3-D Numerical Solutions of Maxwell Equations," *IEEE Trans. Geosci. Remote Sens.*, vol. 42, no. 8, pp. 1739-1748, Aug. 2004.

[7] N. Nakashima, S. Fujino, and M. Tateiba, "Performance Evaluation of State-of-the-Art Linear Iterative Solvers Based on IDR Theorem for Large Scale Electromagnetic Multiple Scattering Simulations," *Appl. Comput. Electromagn. Soc. J.*, vol. 26, no. 1, pp. 37-44, Jan. 2011.

[8] C.-H. Kuo and M. Moghaddam, "Scattering from Multilayer Rough Surfaces Based on the Extended Boundary Condition Method and Truncated Singular Value Decomposition," *IEEE Trans. Antennas Propag.*, vol. 54, no. 10, pp. 2917-2929, Oct. 2006.

[9] C. D. Moss, T. M. Grzegorczyk, H. C. Han, and J. A. Kong, "Forward-Backward Method with Spectral Acceleration for Scattering from Layered Rough Surfaces," *IEEE Trans. Antennas Propag.*, vol. 54, no. 3, pp. 1006-1016, Mar. 2006.

[10] M. El-Shenawee, "Polarimetric Scattering from Two-Layered Two-Dimensional Random Rough Surfaces With and Without Buried Objects," *IEEE Trans. Geosci. Remote Sens.*, vol. 42, no. 1, pp. 67-76, Jan. 2004.

[11] N. Déchamps, N. De Beaucoudrey, C. Bourlier, and S. Toutain, "Fast Numerical Method for Electromagnetic Scattering By Rough Layered Interfaces: Propagation-Inside-Layer Expansion Method," *J. Opt. Soc. Am. A*, vol. 23, no. 2, pp. 359-369, Feb. 2006.

[12] Z. N. Jiang, Z. H. Fan, D. Z. Ding, R. S. Chen, and K. W. Leung, "Preconditioned MDA-SVD-MLFMA for Analysis of Multi-Scale Problems," *Appl. Comput. Electromagn. Soc. J.*, vol. 25, no. 11, pp. 914-925, Nov. 2010.

[13] M. El-Shenawee, C. Rappaport, D. Jiang, W. Meleis, and D. Kaeli, "Electromagnetics Computations using the MPI Parallel Implementation of the Steepest Descent Fast Multipole Method (SDFMM)," *Appl. Comput. Electromagn. Soc. J.*, vol. 17, no. 2, pp. 112-122, Jul. 2002.

[14] S. Tian, Z. Li, C. Q. Gu, and D. P. Ding, "Equivalent Electromagnetic Currents on Infinite Stratified Homogeneous Bi-Anisotropic Media Backed by a PEC Layer," *Appl. Comput. Electromagn. Soc. J.*, vol. 26, no. 3, pp. 206-216, Mar. 2011.

[15] L. Tsang, C. H. Chan, K. Park, and H. Sangani, "Monte-Carlo Simulations of Large-Scale Problems of Random Rough Surface Scattering and Applications to Grazing Incidence with the BMIA/Canonical Grid Method," *IEEE Trans. Antennas Propag.*, vol. 43, no. 8, pp. 851-859, Aug. 1995.

[16] C. H. Chan, L. Tsang, and Q. Li, "Monte Carlo Simulation of Large-Scale One-Dimensional Random Rough-Surface Scattering at Near-Grazing Incidence: Penetrable Case," *IEEE Trans. Antennas Propag.*, vol. 46, no. 1, pp. 142-149, Jan. 1998.

[17] N. Déchamps, and C. Bourlier, "Electromagnetic Scattering from a Rough Layer: Propagation-Inside-Layer Expansion Method Combined to an Updated BMIA/CAG Approach," *IEEE Trans. Antennas Propag.*, vol. 55, no. 10, pp. 2790-2802, Oct. 2007.

[18] L. Tsang, J. A. Kong, K.-H. Ding, and C. O. Ao, *Scattering of Electromagnetic Waves: Numerical Simulations*, Wiley, New York, 2001.

[19] K. F. Warnick and W. C. Chew, "Numerical Simulation Methods for Rough Surface Scattering," *Waves Random Media*, vol. 11, no. 1, pp. R1-R30, Jan, 2001.

[20] T. Kobayashi, H. Oya, and T. Ono, "A-Scope Analysis of Subsurface Radar Sounding of Lunar Mare Region," *Earth Planets Space*, vol. 54, no. 10, pp: 973-982, Oct. 2002.

[21] Y. Du and J. A. Kong, "Application of Stochastic Second-Degree Method to Electromagnetic Scattering from Randomly Rough Surfaces,"

Electron. Lett., vol. 43, no. 23, pp. 1244-1246, Nov. 2007.

[22] K. Pak, L. Tsang, and J. Johnson, "Numerical Simulations and Backscattering Enhancement of Electromagnetic Waves from Two-Dimensional Dielectric Random Rough Surfaces with the Sparse-Matrix Canonical Grid Method," *J. Opt. Soc. Am. A*, vol. 14, no. 7, pp. 1515-1529, Jul. 1997.

[23] E. I. Thorsos, "The Validity of the Kirchhoff Approximation for Rough Surface Scattering using a Gaussian Roughness Spectrum," *J. Acous. Soc. Am.*, vol. 83, no. 1, pp. 78-92, Jan. 1988.

[24] Z. G. Meng, S. B. Chen, E. Osei, Z. J. Wang, and T. F. Cui, "Research on Water Ice Content in Cabeus Crater using the Data from the Microwave Radiometer OnBoard Chang'e-1 Satellite," *Sci. China Phys. Mech. Astron.*, vol. 53, no. 12, pp: 2172-2178, Dec. 2010.

Linfeng He received the B.S., and M.S. in Department of Electronics and Information, Huazhong University of Science and Technology, Wuhan, China, in 2006, 2008, respectively. He is presently a Ph.D. candidate in the Department of Electronics and Information, Huazhong University of Science and Technology, Wuhan, China. His research interests include microwave remote sensing, and computational electromagnetics.

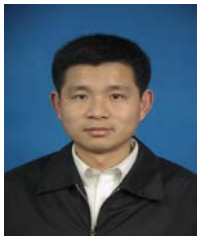

Liang Lang received the Ph.D. degree in the Electromagnetic Field and Microwave Technology from Huazhong University of Science and Technology, Wuhan, China, in 2009. He is presently an associate professor in the Department of Electronics and Information Engineering, Huazhong University of Science and Technology. The focus of his research was electromagnetic simulations and microwave remote sensing.

Qingxia Li received the B.S., M.S., and Ph.D. degree in Department of Electronics and Information, Huazhong University of Science and Technology, Wuhan, China, in 1987, 1990, 1999, respectively. He is presently a professor in the Department of Electronics and Information, Huazhong University of Science and Technology, Wuhan, China. His research interests include microwave remote sensing, electromagnetics, and antenna array.

Wenchao Zheng received the B.S. from Xi'an institute of Posts and Telecommunications, Xi'an, China, in 2008 and the M.S. from Wuhan Research institute of Posts and Telecommunications, Wuhan, China in 2011. He is currently working toward the Ph.D. degree in Huazhong University of Science and Technology, Wuhan, China. His research interests include microwave remote sensing and scattering of electromagnetic waves.